RSC Advances

PAPER

View Article Online
View Journal | View Issue

Cite this: *RSC Adv.*, 2024, **14**, 7234

Adsorption mechanism of Ca^{2+}, Mg^{2+}, Fe^{3+}, and Al^{3+} ions in phosphoric acid–nitric acid solution on 001 × 7 and S957 resins

Yingyuan Hu,[a] Wenlong Zhang,[a] Meizhao Xue,[a] Rui Lv, *[b] Caimei Fan[b] and Ao Li*[bc]

Selective removal of Ca^{2+} and Mg^{2+} ions using the 001 × 7 resin and Fe^{3+} and Al^{3+} ions using the S957 resin is able to achieve the deep purification of the phosphoric acid–nitric acid solution, but the adsorption behaviors of Fe^{3+} and Al^{3+} ions are seriously suppressed by phosphoric acid. In order to understand the interaction mechanism of separation processes and the influence of phosphoric acid, we first studied the bonding form of Ca^{2+}, Mg^{2+}, Fe^{3+}, and Al^{3+} ions on 001 × 7 and S957 resins using FT-IR and XPS techniques; subsequently, quantum chemistry computation was carried out to further explore the bonding mechanism between the functional groups on resins and metal ions. FT-IR and XPS results reveal that for the adsorption process on the 001 × 7 resin, hydroxyls from sulfonic acid groups combine with Ca^{2+} and Mg^{2+} ions. Whereas Fe^{3+} and Al^{3+} ions are adsorbed on the S957 resin through an exchange reaction with hydroxyls on the phosphonic acid group but not on the sulfonic acid group. Quantum chemistry computation results reveal that the phosphonic acid group has a larger binding energy with Fe^{3+} and Al^{3+} ions. Thus, the S957 resin still presents great adsorption performance for Fe^{3+} and Al^{3+} ions despite the influence of dihydrogen phosphate ions in the phosphoric acid–nitric acid solution.

Received 23rd December 2023
Accepted 16th February 2024

DOI: 10.1039/d3ra08791c

rsc.li/rsc-advances

1 Introduction

Phosphoric acid–nitric acid solution is the neutralization mother liquor obtained using the nitric acid resolve phosphate ore, which can be used to produce nitrogen and phosphorus compound fertilizers.[1,2] In addition to phosphoric acid (4.4 mol L^{-1}) and nitric acid (1.1 mol L^{-1}), this solution contains many Ca^{2+} ions (1.9 mol L^{-1}) and a few Mg^{2+}, Fe^{3+}, and Al^{3+} ions (0.14–0.24 mol L^{-1}). During the neutralization process, the presence of these metal ions leads to the formation of precipitates in the phosphoric acid–nitric acid solution, which makes the solution easily viscous and water-soluble phosphorus degenerate.[3–5] In order to alleviate such problems, a precipitation method is usually used to remove most of the Ca^{2+} ions from phosphoric acid–nitric acid solution in industry.[6] But limited by the solubility of metal ions, a small amount of Ca^{2+} ions still remain in the solution,[7] and Mg^{2+}, Fe^{3+}, and Al^{3+} ions also are not removed. Therefore, the in-depth removal of these small four metal ions from the mother liquor is essential for practical production.

Synthetic resins have been proven to effectively remove Ca^{2+}, Mg^{2+}, Fe^{3+}, and Al^{3+} ions from phosphoric acid–nitric acid solution. Ca^{2+} and Mg^{2+} ions can be selectively removed by the 001 × 7 resin (containing a sulfonic acid group),[8] and Fe^{3+} and Al^{3+} ions are selectively removed by the S957 resin (containing a sulfonic acid group and phosphonic acid group).[9] Metal ions adsorbed on the 001 × 7 resin and S957 resin can be completely eluted with nitric acid and hydrochloric acid as regeneration solutions, respectively, achieving the recycling utilization of resins. Nevertheless, very little attention has been paid to the interaction mechanism of separation processes and the adsorption mechanism of the four metal ions from phosphoric acid–nitric acid solution using different resins.

Furthermore, it should be noted that the 001 × 7 resin presents great adsorption capacity for Fe^{3+} and Al^{3+} ions in pure water or nitric acid solution, while no adsorption capacity is observed in phosphoric acid solution.[10] Adsorption capacity of S957 resin for Fe^{3+} and Al^{3+} ions also decrease significantly with the concentration of phosphoric acid increasing. Consequently, phosphoric acid has a particular influence on the adsorption process of Fe^{3+} and Al^{3+} ions on resins. Much work has been performed so far on the adsorption process of metal ions on resins and the influence of the coexisting component.[11,12] It is believed that the dissociated phosphoric acid anion can combine with metal ions to form the phosphate chelate and suppress its adsorption behavior on the resin. However, there are relatively few studies devoted to proving this influencing

[a]*College of Traditional Chinese Medicine and Food Engineering, Shanxi University of Chinese Medicine, Jinzhong, 030619, China*

[b]*College of Safety and Emergency Management and Engineering, Taiyuan University of Technology, Taiyuan, 030024, China. E-mail: lvrui5276@163.com; everliao007@qq.com*

[c]*Jinneng Holding Group, Datong 037000, Shanxi, China*

mechanism from a microscopic view. Further effort on the adsorption mechanism is required to understand the effect of phosphoric acid.

Recent research efforts by the characterization of resin to explore the removal mechanism of metal ions from phosphoric acid have attracted much attention.[13,14] Based on modern spectroscopic characterizations, such as Fourier transform infrared spectra (FT-IR) and X-ray photoelectron spectra (XPS), variation in the chemical components, elemental valence states and functional groups of resins (fresh, adsorbed metal ions, and regenerated) can be obtained and used to infer the bonding forms of the metal ion on the resin. Besides, density functional theory (DFT) calculation is a powerful theoretical tool that can provide effective evidence for the interaction mechanism of the microstructures.[15,16] Thus, further quantum chemical calculation about the binding energies of metal ions with functional groups on the resins and phosphate anion in phosphoric acid solution will supply the theoretical support for the adsorption mechanism.

Therefore, in this study, we firstly focused on the adsorption mechanism for removal of Ca^{2+}, Mg^{2+}, Fe^{3+}, and Al^{3+} ions from the phosphoric acid–nitric acid solution by 001 × 7 and S957 resins, using BET, FT-IR and XPS characterization techniques to investigate and compare the microstructure of resins before and after metal ions adsorption, and after metal ions elution. Furthermore, using chemical structures of 001 × 7 resin, S957 resin and dihydrogen phosphate ion as molecular models, quantum chemistry calculations about the binding energies of metal ions with the functional group on the resin and phosphate anions in the phosphoric acid solution were carried out to explore the bonding mechanism between the functional groups and metal ions and provide a theoretical basis for the adsorption mechanism of Ca^{2+}, Mg^{2+}, Fe^{3+}, and Al^{3+} ions from phosphoric acid–nitric acid solution on 001 × 7 and S957 resins.

2 Experimental section

2.1. Materials and chemicals

Strong acid cation resin 001 × 7 and chelating resin S957 were obtained from Fuchen Chemical Reagent Factory and Purolite (China) Co., Ltd., respectively, and their characteristics were listed in Table 1. Analytical grade $Ca(NO_3)_2 \cdot 4H_2O$, $Mg(NO_3)_2 \cdot 6H_2O$, $Fe(NO_3)_3 \cdot 9H_2O$, $Al(NO_3)_3 \cdot 9H_2O$, and 65 wt% HNO_3, 85 wt% H_3PO_4, 36 wt% HCl were used to prepare the synthetic solutions and the regeneration solutions, respectively.

2.2. Dynamic adsorption and elution

Dynamic adsorption and elution processes were carried out in a glass column (internal diameter: 2 cm, length: 25 cm). The flow rate was controlled at 1 mL min^{-1} using a peristaltic pump (SHENCHEN, Lab 2015). The operations were performed as follows:

(a) Synthetic resin (001 × 7 or S957) was firstly loaded into the column, then the deionized water was fed from the top of the column to rinse the resin. The resin in the column was collected as the sample of the resin before the adsorption of metal ions.

(b) Phosphoric acid–nitric acid solutions (4.4 mol L^{-1} phosphoric acid and 1.1 mol L^{-1} nitric acid) containing 0.25 mol L^{-1} Ca^{2+} and Mg^{2+} ions, or 0.15 mol L^{-1} Fe^{3+} and Al^{3+} ions were prepared according to the typical compositions of the neutralization mother liquor obtained from the Chemical Group Co. Ltd of China.[10] The prepared solution passed through the column in the upflow mode. After the end of the adsorption process, the deionized water was fed from the top of the column to rinse the phosphoric acid–nitric acid solution retained. The resin in the column was collected as the sample of the resin after the adsorption of metal ions.

(c) The regeneration solution (7 mol L^{-1} nitric acid solution or 8 mol L^{-1} hydrochloric acid solution) was flown through the column upward. After the end of the elution process, the deionized water was fed from the top of the column to rinse the regeneration solution retained. Resin in the column was collected as the sample of the resin after the elution of metal ions.

2.3. Characterization

FT-IR spectra were recorded on a Shimadzu-8400 spectrometer in the range of 400–4000 cm^{-1} using KBr pellets. XPS spectra measurements were performed on a Thermo ESCALAB 250 with an Al Kα beam spot source ($h\nu$ = 1486.6 eV, 150 W, 500 μm). The shift in the binding energy caused by the relative surface charges was referenced to the C 1s peak (284.8 eV) of the surface adventitious carbon. The surface area, pore volume, and pore size of the resin were measured by nitrogen adsorption–desorption isotherms using a Micromeritics ASAP-2460 instrument.

Table 1 Characteristics of the 001 × 7 resin and S957 resin supplied by the manufacturer

Characteristics	001 × 7 resin	S957 resin
Polymer structure	Gel-type polystyrene crosslinked with divinylbenzene	Macroporous polystyrene crosslinked with divinylbenzene
Functional groups	Sulfonic acid	Phosphonic acid and sulfonic acid
Ionic form	Na^+	H^+
Total exchange capacity	≥1.8 equiv. L^{-1}	18 g L^{-1} (iron capacity)
Specific gravity	1.23–1.28	1.12
Moisture holding capacity	45–55%	55–70%
Particle size	0.3–1.2 mm	0.3–0.8 mm
Operating temperature	100 °C	90 °C
pH range	1–14	1–14

2.4. Quantum chemistry computation

DFT calculations were run using the Gaussian 16 program package to comprehend the interaction mechanism of the metal ions with the resins. All the molecular structures in this study were built using Chem3D. The geometry optimizations and energy calculations were performed at the 6-31G(d) level of theory using the B3LYP method. The binding energies were calculated as follows:[15–17]

$$\Delta E = E_{(\text{adsorbent-metal ion complex})} - E_{(\text{adsorbent})} - E_{(\text{metal ion})} \quad (1)$$

in which, $E_{(\text{adsorbent-metal ion complex})}$ is the energy of the adsorbent-metal ion complex (hartree), $E_{(\text{adsorbent})}$ is the energy of the adsorbent (hartree), and $E_{(\text{metal ion})}$ is the energy of the metal ion (hartree).

3 Results and discussion

3.1. Adsorption mechanism on 001 × 7 resin

Fig. 1 presents the FT-IR spectra of 001 × 7 resins before and after the adsorption of Ca^{2+}, Mg^{2+} ions, and after the elution of Ca^{2+}, Mg^{2+} ions. The peaks around 3363–3523 cm^{-1} are assigned to the O–H stretching vibration of water absorbed and the sulfonic acid group.[18–20] The peaks at 1181 and 1036 cm^{-1} are ascribed to S=O asymmetric stretching vibration and symmetric stretching vibration of the sulfonic acid group, respectively.[21,22] It can be observed from Fig. 1 that after the adsorption of Ca^{2+} and Mg^{2+} ions, the intensity of the characteristic peaks of O–H weakens, while the characteristic peaks of S=O are unchanged. After the elution of metal ions through nitric acid, the characteristic peaks of O–H recover and are almost the same as those before the adsorption of metal ions. These results reveal that during the adsorption process of Ca^{2+} and Mg^{2+} ions on 001 × 7 resin, the hydroxyl group on the sulfonic acid group combines with metal ions; meanwhile, the H^+ ion is released, and after the regeneration with nitric acid, the hydroxyl is restored through the exchange reaction between the H^+ ion at a higher concentration and the metal ion.

XPS spectra of 001 × 7 resins are shown in Fig. 2. The peaks centered at the binding energy of 347.4 eV and 351.0 eV correspond to Ca $2p_{3/2}$ and Ca $2p_{1/2}$, respectively.[23,24] The peak of Mg 1s centers at the binding energy of 1304.8 eV.[25,26] The spectrum of O 1s can be divided into two peaks centered at 531.3 eV and 532.8 eV, which are associated with O=S and O–H, respectively.[27] The spectrum of S 2p can be split into two peaks S $2p_{3/2}$ (167.8 eV) and S $2p_{1/2}$ (169.0 eV), which are assigned to S–O and S=O, respectively.[28]

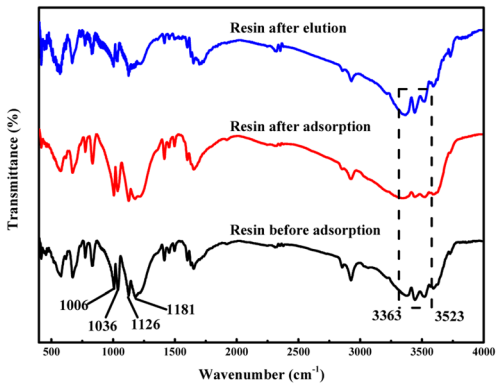

Fig. 1 FT-IR spectra of 001 × 7 resins before and after the adsorption of Ca^{2+} and Mg^{2+} ions, and after the elution of Ca^{2+} and Mg^{2+} ions.

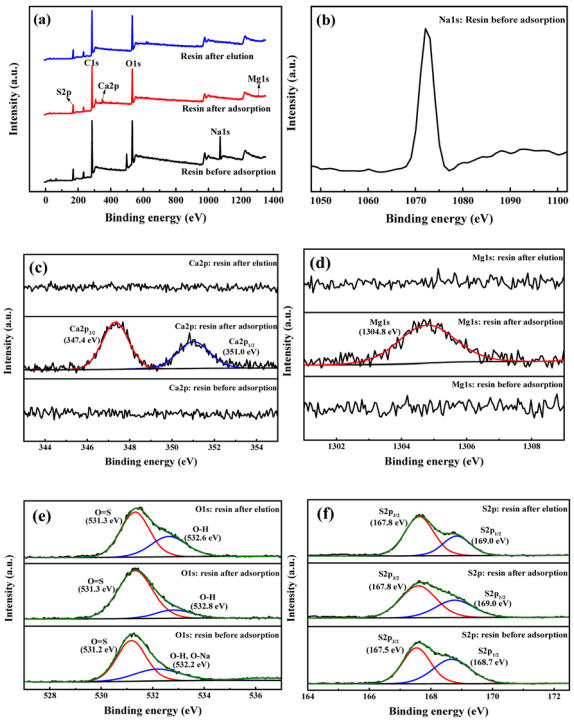

Fig. 2 XPS spectra of 001 × 7 resins before and after the adsorption of Ca^{2+} and Mg^{2+} ions and after the elution of Ca^{2+}, Mg^{2+} ions: (a) survey, (b) Na 1s, (c) Ca 2p, (d) Mg 1s, (e) O 1s, and (f) S 2p.

As shown in Fig. 2(a) and (b), due to the presence of the Na-type sulfonic acid group, XPS spectra of the fresh 001 × 7 resin exhibit Na 1s peak.[29–31] After the adsorption of Ca^{2+} and Mg^{2+} ions, Na 1s peak disappears, while Ca $2p_{3/2}$, Ca $2p_{1/2}$ peaks and the Mg 1s peak appear. As a result of the exchange reaction between Ca^{2+} and Mg^{2+} ions and the H^+ ion on the hydroxyl of the sulfonic acid group, the peak at the binding energy of 532.8 eV weakens, and the swell in the spectrum of S 2p for S=O almost disappears. After the of elution metal ions by nitric acid, Na 1s peak, Ca $2p_{3/2}$, Ca $2p_{1/2}$ peaks, and the Mg 1s peak disappear, which reveals that the Ca^{2+} and Mg^{2+} ions adsorbed on 001 × 7 resin are completely eluted and all of the sulfonic acid groups are H-type. In addition, the peak at the binding energy of 532.8 eV for O–H is enhanced, and the swell in the spectrum of S 2p for S=O is the same as in the spectrum before adsorption.

3.2. Adsorption mechanism on S957 resin

Fig. 3 presents FT-IR spectra of S957 resin before and after the adsorption of Fe^{3+} and Al^{3+} ions and after the elution of Fe^{3+} and Al^{3+} ions. Apparently, after the adsorption of Fe^{3+} and Al^{3+} ions,

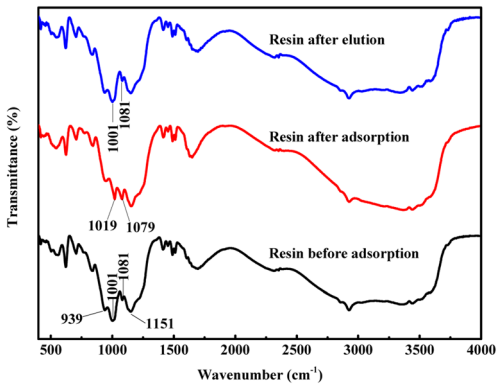

Fig. 3 FT-IR spectra of S957 resin before and after the adsorption of Fe^{3+} and Al^{3+} ions, and after the elution of Fe^{3+}, and Al^{3+} ions.

the characteristic peak at 1001 cm^{-1} shifts to 1019 cm^{-1}, and the peak intensity weakens, while the characteristic peak at 1081 cm^{-1} shifts to 1079 cm^{-1} and the peak intensity strengthens. However, because the characteristic peaks of the phosphonic acid group and sulfonic acid group are centered at 900–1200 cm^{-1},[32–34] it is difficult to understand the bonding mechanism of Fe^{3+} and Al^{3+} ions with functional groups on S957 resin from its FT-IR spectra. Nevertheless, after the metal ions are eluted by hydrochloric acid, the characteristic peaks at 1001 cm^{-1} and 1081 cm^{-1} are recovered, and are almost the same as those before metal ion adsorption. This reveals that Fe^{3+} and Al^{3+} ions adsorbed on S957 resin are eluted successfully and functional groups are recovered.

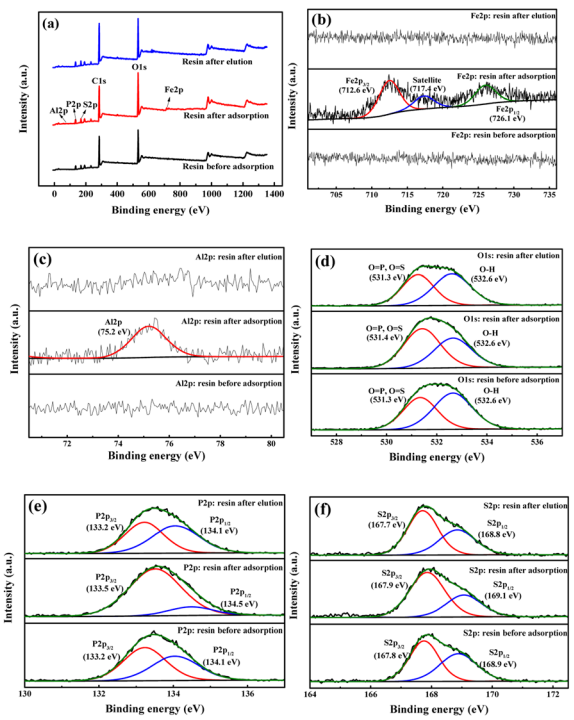

Fig. 4 XPS spectra of S957 resins before and after the adsorption of Fe^{3+} and Al^{3+} ions, and after the elution of Fe^{3+} and Al^{3+} ions: (a) survey, (b) Fe 2p, (c) Al 2p, (d) O 1s, (e) P 2p, and (f) S 2p.

XPS spectra of S957 resin are shown in Fig. 4. The peaks centered at the binding energy of 712.6 eV and 726.1 eV correspond to Fe $2p_{3/2}$ and Fe $2p_{1/2}$, respectively, while the satellite peak of Fe $2p_{3/2}$ indicates binding energy of 717.4 eV.[35–37] The peak of Al 2p centers at the binding energy of 75.2 eV.[38–40] The spectrum of O 1s can be divided into two peaks centered at 531.3 eV (O═P and O═S) and 532.8 eV (O–H).[41] The spectrum of P 2p can be divided into two peaks centered at 133.2 eV (P $2p_{3/2}$) and 134.1 eV (P $2p_{1/2}$), which are associated with P═O and P–O, respectively.[42,43] The spectrum of S 2p can be split into two peaks at 167.8 eV (S 2p3/2) and 168.9 eV (S 2p1/2).

It can be observed from the XPS spectra of S957 resin that after the adsorption of Fe^{3+} and Al^{3+} ions, peaks of Fe $2p_{3/2}$, Fe $2p_{1/2}$, and Al 2p appear, and the peaks of O–H at the binding energy of 532.6 eV and P–O at the binding energy of 134.5 eV weaken, while the peaks of S 2p are almost unchanged. These results indicate that Fe^{3+} and Al^{3+} ions are adsorbed on S957 resin through the exchange reaction with H^+ ions from the phosphonic acid group but not from the sulfonic acid group. After the metal ion elution, peaks for Fe $2p_{3/2}$, Fe $2p_{1/2}$ and Al 2p disappeared, and the peaks of O–H at the binding energy of 532.6 eV and P–O at the binding energy of 134.5 eV are enhanced, and are the same in comparison to the spectra before adsorption.

3.3. Bonding mechanism between functional groups on the resin and metal ions

Quantum chemistry computation about the binding energies of different adsorbents (sulfonic acid group, phosphonic acid group, and dihydrogen phosphate ion) with Ca^{2+}, Mg^{2+}, Fe^{3+}, and Al^{3+} ions was carried out to explore the bonding mechanism of the metal ions in phosphoric acid solution with functional groups on the resins. Based on the FT-IR and XPS spectra of 001 × 7 resins and S957 resins, adsorbent of the sulfonic acid group is built by structural units of 001 × 7 resin, in which sulfonic acid group loses the movable hydrogen ion, while adsorbent of the phosphonic acid group is built by the structural unit of S957 resin, in which phosphonic acid group loses a movable hydrogen ion and sulfonic acid group does not. Conformations of different adsorbents are shown in Fig. 5.

Optimized conformations of the adsorbent-metal ion complexes are presented in Fig. 6–8. The binding energies of adsorbent-metal ion complexes are listed in Table 2. It can be observed that the differences in the binding energies of the sulfonic acid group-metal ion complexes and dihydrogen

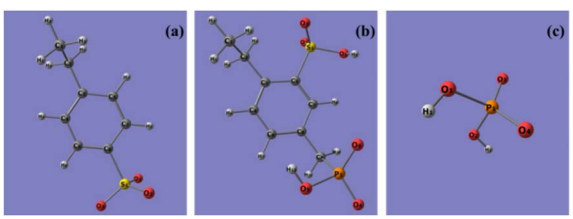

Fig. 5 Conformations of different adsorbents, (a) sulfonic acid group, (b) phosphonic acid group, and (c) dihydrogen phosphate ion.

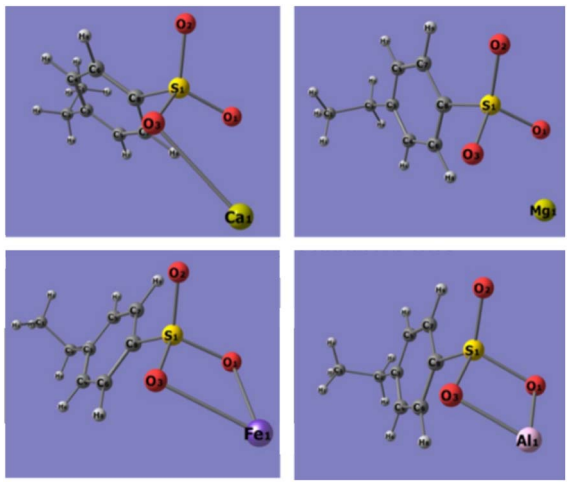

Fig. 6 Optimized conformations of sulfonic acid group-metal ion complexes.

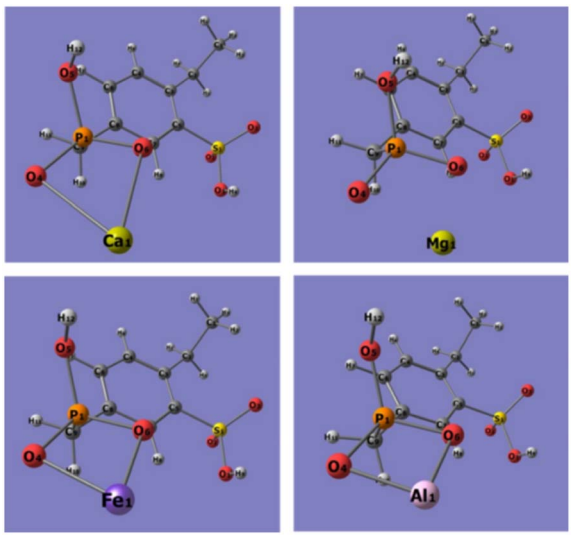

Fig. 7 Optimized conformations of phosphonic acid group-metal ion complexes.

phosphate ion-metal ion complexes are 19.1662, 34.1315, 73.2515, and 98.7188 kJ mol^{-1} (Ca^{2+}, Mg^{2+}, Fe^{3+}, and Al^{3+} ions, respectively). This indicates that dihydrogen phosphate ion has stronger binding energy to metal ions, and the differences in the binding energies of the two adsorbents with Ca^{2+} and Mg^{2+} ions are smaller, but the differences with Fe^{3+} and Al^{3+} ions are larger. Accordingly, under the influence of dihydrogen phosphate ion in the phosphoric acid solution, 001 × 7 resin containing only the sulfonic acid groups presents the adsorption ability to Ca^{2+} and Mg^{2+} ions while worse adsorption performance is seen for Fe^{3+} and Al^{3+} ions. Due to the weaker binding ability of the sulfonic acid group with Fe^{3+} and Al^{3+} ions, when Fe^{3+} and Al^{3+} ions in the phosphoric acid solution are adsorbed on the S957 resin, this group does not combine with Fe^{3+} and Al^{3+} ions.

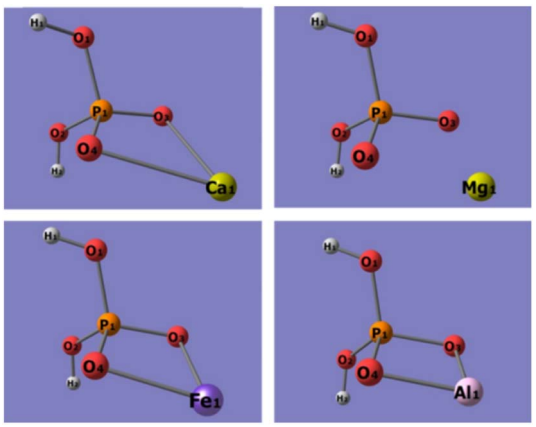

Fig. 8 Optimized conformations of dihydrogen phosphate ion-metal ion complexes.

On the other hand, the differences in the binding energies of phosphonic acid group-metal ion complexes and dihydrogen phosphate ion-metal ion complexes are 3.1506, −4.2008, −16.2781, and −43.8459 kJ mol^{-1} (Ca^{2+}, Mg^{2+}, Fe^{3+}, and Al^{3+} ions, respectively). That is, compared with the phosphonic acid group, the dihydrogen phosphate ion has stronger binding energy to the Ca^{2+} ion, while weaker binding energies for Mg^{2+}, Fe^{3+}, and Al^{3+} ions. Therefore, S957 resin containing the phosphonic acid group can hold great adsorption ability towards Fe^{3+} and Al^{3+} ions in the phosphoric acid solution, due to their higher binding performance with the phosphonic acid group while lower binding performance with the dihydrogen phosphate ion.

Thus, it can be concluded that due to the strong binding ability of the dihydrogen phosphate ions with Fe^{3+} and Al^{3+} ions, their adsorption behavior on the resin will be seriously affected by the coexisting phosphoric acid. Based on the order of the binding energy between the two metal ions and the adsorbent molecule: phosphonic acid group > dihydrogen phosphate ions > sulfonic acid group, the adsorption ability of 001 × 7 resin only containing sulfonic group to Fe^{3+} and Al^{3+} ions is very poor under the influence of dihydrogen phosphate ions dissociating from phosphoric acid, while S957 resin containing sulfonic acid group/phosphonic acid group has good adsorption capacity. Therefore, the coexisting components possessing strong binding ability with metal ions have a significant impact on their adsorption behaviors on the resins. Only the resin containing a strong binding ability functional group has the adsorption performance. Therefore, in order to further improve the separation efficiency of Fe^{3+} and Al^{3+} ions in the phosphoric acid solution, an important modification method is immobilizing a more efficient functional group on the resin, such as increasing the ratio of the phosphonic acid group and sulfonic acid group. The relevant modification experiments for the resins with different amounts of the phosphonic acid group and sulfonic acid group and their adsorption ability for Fe^{3+} and Al^{3+} ions from phosphoric acid solution are being studied in our laboratory.

Table 2 Binding energies of different adsorbent-metal ion complexes

$E_{(\text{metal ion})}$/hartree	$E_{(\text{adsorbent})}$/hartree		$E_{(\text{adsorbent-metal ion complex})}$/hartree	ΔE/hartree	ΔE/kJ mol^{-1}
−677.5218 (Ca^{2+})	$-SO_3^-$	−934.4345	−1611.9707	−0.0144	−37.8072
	$-PO_3H^-$	−1541.5626	−2219.1049	−0.0205	−53.8227
	$H_2PO_3^-$	−643.8381	−1321.3816	−0.0217	−56.9733
−199.8449 (Mg^{2+})	$-SO_3^-$	−934.4345	−1134.3397	−0.0603	−158.318
	$-PO_3H^-$	−1541.5626	−1741.4824	−0.0749	−196.65
	$H_2PO_3^-$	−643.8381	−843.7563	−0.0733	−192.449
−1263.2078 (Fe^{3+})	$-SO_3^-$	−934.4345	−2197.6961	−0.0538	−141.252
	$-PO_3H^-$	−1541.5626	−2804.8583	−0.0879	−230.781
	$H_2PO_3^-$	−643.8381	−1907.1276	−0.0817	−214.503
−241.4268 (Al^{3+})	$-SO_3^-$	−934.4345	−1176.2687	−0.4074	−1069.63
	$-PO_3H^-$	−1541.5626	−1783.4511	−0.4617	−1212.19
	$H_2PO_3^-$	−643.8381	−885.7099	−0.4450	−1168.35

3.4. Influence of resin's porous structure

In order to further understand the adsorption mechanism, the adsorption processes of Ca^{2+}, Mg^{2+}, Fe^{3+}, and Al^{3+} ions on D001 resin were carried out to explore the influence of the resin porous structure. According to resin characteristics supplied by the manufacturer, the D001 resin contains the same functional group as the 001 × 7 resin, but its polymer structure is macroporous polystyrene crosslinked with divinylbenzene, rather than the gel-type. As shown in the nitrogen adsorption–desorption isotherms of different resins (Fig. 9), the curves of D001 resin and S957 resin have smaller variations at $P/P_0 < 0.1$, while upward tendency in $0.1 < P/P_0 < 0.8$. This indicates that the two resins contain mesoporous structures but do not contain microporous structures. Specific surface area, pore volume, and average pore size of D001 resin and S957 resin are 3.67 and 3.44 $m^2\ g^{-1}$, 0.04 and 0.03 $cm^3\ g^{-1}$, 36.35 and 48.80 nm, respectively. On the other hand, the amount of N_2 adsorbed on the 001 × 7 resin at $0 < P/P_0 < 1.0$ is almost 0 $cm^3\ g^{-1}$. This phenomenon is because the gel-type 001 × 7 resin only generates a microporous structure after absorbing water and swelling, but this kind of porous structure is very small, and the specific surface area and pore structure parameters of the 001 × 7 resin could not be obtained from the test results.

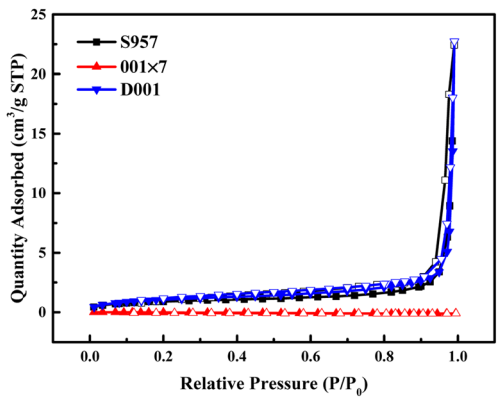

Fig. 9 Nitrogen adsorption–desorption isotherms of S957 resin, 001 × 7 resin, and D001 resin.

Batch adsorption experiments indicate that the equilibrium adsorption capacities of D001 resin to Ca^{2+}, Mg^{2+}, Fe^{3+}, and Al^{3+} ions in the phosphoric acid–nitric acid solution are 0.97, 0.71, 0.02, and 0.18 mmol g^{-1}, respectively, which are almost the same with those of 001 × 7 resin (0.96, 0.74, 0.02, and 0.20 mmol g^{-1}, respectively). Accordingly, it can be concluded that D001 resin and 001 × 7 resin have the same adsorption performances as the four metal ions in the phosphoric acid–nitric acid solution, thus the key factors in the adsorption ability of the resin are not the porous structure parameters but the functional groups on it.

4 Conclusions

We studied the adsorption mechanism of Ca^{2+}, Mg^{2+}, Fe^{3+}, and Al^{3+} ions on 001 × 7 and S957 resins using FT-IR and XPS characterization techniques and quantum chemistry computation between the functional groups and metal ions. Results reveal that the adsorption mechanism of the 001 × 7 resin is the ion exchange reaction between the hydroxyl on the sulfonic acid group and Ca^{2+}, Mg^{2+} ions. The adsorption mechanism of the S957 resin involves the ion exchange reaction between hydroxyl on the phosphonic acid group and Fe^{3+}, Al^{3+} ions, while the sulfonic acid group and porous structural parameters have little influence. Quantum chemistry computation results reveal that the strong binding ability of dihydrogen phosphate ions to Fe^{3+} and Al^{3+} ions makes their adsorption behavior on the resin affected seriously by the coexisting phosphoric acid. As a consequence, only the resin containing a strong binding ability functional group, such as the phosphonic acid group, has the adsorption performance for Fe^{3+} and Al^{3+} ions from the phosphoric acid solution.

Author contributions

Yingyuan Hu: conceptualization, methodology, writing – original draft, writing – review and edition. Wenlong Zhang: methodology, supervision. Meizhao Xue: investigation, data curation. Rui Lv: methodology, data curation, resources, supervision. Caimei Fan: methodology, supervision. Ao Li: investigation, data curation.

Conflicts of interest

There are no conflicts to declare.

Acknowledgements

This work was sponsored by the Natural Science Foundation for Young Scientists of Shanxi Province (No. 202103021223111, No. 202203021212347), Doctoral Research Start-up Fund (No. 2020BK08) and Scientific and Technological Innovation Capacity Cultivation Program (2023PY-TH-04) of Shanxi University of Chinese Medicine, Jinneng Coal Industry Group Co., Ltd. and Taiyuan University of Technology Postdoctoral project (No. 275226).

Notes and references

1 X. L. Yin, S. W. Tang, T. Zhang, Y. He and L. Lv, *Ind. Eng. Chem. Res.*, 2023, **62**, 6311–6321.
2 D. H. Xu, B. H. Zhong, X. L. Wang, X. Li, Y. J. Zhong, Z. J. Yan, J. X. Yang, X. B. Li, Y. M. Wang and X. H. Zhou, *Chinese J. Chem. Eng.*, 2022, **41**, 170–175.
3 G. R. Campbell, Y. K. Leong, C. C. Berndt and J. L. Liow, *Chem. Eng. Sci.*, 2006, **61**, 5856–5866.
4 J. Ando and J. R. Lehr, *J. Agric. Food. Chem.*, 1968, **16**, 391–398.
5 J. C. Brosheer and F. A. Lenfesty, *J. Agric. Food. Chem.*, 1958, **6**, 827–833.
6 H. J. Jing, X. X. Zheng, C. M. Fan, J. Q. Feng, Y. F. Wang and G. Y. Ding, *Adv. Mater. Res.*, 2011, **146**, 1066–1069.
7 Y. Zhang and M. Muhammed, *J. Chem. Eng. Data*, 1989, **34**(1), 121–124.
8 R. Lv, Q. Xi, T. Li, R. Li, X. C. Zhang, J. X. Liu, C. M. Fan, J. Q. Feng, L. Y. Zhang and Z. H. Wang, *Chinese J. Chem. Eng.*, 2019, **27**, 2930–2936.
9 R. Lv, Y. Y. Hu, Z. H. Jia, R. Li, X. C. Zhang, J. X. Liu, C. M. Fan, J. Q. Feng, L. Y. Zhang and Z. H. Wang, *Ind. Eng. Chem. Res.*, 2019, **58**, 21641–21648.
10 R. Lv, Y. Y. Hu, Z. H. Jia, R. Li, X. C. Zhang, J. X. Liu, C. M. Fan, J. Q. Feng, L. Y. Zhang and Z. H. Wang, *Hydrometallurgy*, 2019, **188**, 194–200.
11 D. S. Eldridge, R. J. Crawford and I. H. Harding, *J. Colloid Interface Sci.*, 2015, **454**, 20–26.
12 N. Kabay, M. Demircioğlu, H. Ekinci, M. Yüksel, M. Sağlam, M. Akçay and M. Streat, *Ind. Eng. Chem. Res.*, 1998, **37**, 2541–2547.
13 X. K. Leng, Y. J. Zhong, D. H. Xu, X. L. Wang and L. Yang, *Chinese J. Chem. Eng.*, 2019, **27**, 1050–1057.
14 C. L. He, M. W. Qi, Y. Liu, Z. Z. Liu, Y. Z. Wei, T. Fujita, G. F. Wang, S. J. Ma, W. C. Yang and J. Y. Gan, *Hydrometallurgy*, 2024, **224**, 106230.
15 R. Q. Ma, T. Wang, T. B. Huang, W. L. Sun, S. Qiao and W. Liu, *J. Mol. Liq.*, 2020, **312**, 113432.
16 Y. Y. Luo, C. Liu, W. H. Xu and M. G. Shan, *Sep. Purif. Technol.*, 2024, **333**, 125858.
17 D. Tang, Y. L. Zhao, G. J. Xu, T. Yang and D. D. Han, *J. Clean. Prod.*, 2023, **415**, 137651.
18 F. S. Liu, X. L. Ma, H. Li, Y. Y. Wang, P. Cui, M. Guo, H. L. Yaxin, W. P. Lu, S. J. Zhou and M. Z. Yu, *Fuel*, 2020, **266**, 117149.
19 P. B. Zhang, H. Wu, M. M. Fan, W. J. Sun, P. P. Jiang and Y. M. Dong, *Fuel*, 2019, **235**, 426–432.
20 M. Goswami and P. Phukan, *J. Environ. Chem. Eng.*, 2017, **5**, 3508–3517.
21 Z. Z. Lin, M. T. Luo, Y. D. Zhang, X. X. Wu, Y. H. Fu, F. M. Zhang and W. D. Zhu, *Appl. Catal. Gen.*, 2018, **563**, 54–63.
22 T. Wang, C. H. Zhao, J. Xu and D. J. Sun, *Colloid. Surface.*, 2013, **417**, 256–263.
23 Y. F. Chen and X. K. Tang, *Appl. Surf. Sci.*, 2020, **512**, 145663.
24 Y. F. Zhang, Q. S. Wang, S. N. Gao, H. M. Jiang and C. G. Meng, *Micropor. Mesopor. Mat.*, 2018, **266**, 14–23.
25 M. Santamaria, F. D. Quarto, S. Zanna and P. Marcus, *Electrochim. Acta*, 2008, **53**, 1314–1324.
26 S. Ardizzone, C. L. Bianchi, M. Fadoni and B. Vercelli, *Appl. Surf. Sci.*, 1997, **119**, 253–259.
27 M. M. Nasef and H. Saidi, *Appl. Surf. Sci.*, 2006, **252**, 3073–3084.
28 Y. Jin, J. Shi, F. M. Zhang, Y. J. Zhong and W. D. Zhu, *J. Mol. Catal. Chem.*, 2014, **383–384**, 167–171.
29 Z. W. Zhao, Y. X. Song, X. B. Min, Y. J. Liang, L. Y. Chai and M. Q. Shi, *J. Non-Cryst. Solids*, 2016, **452**, 238–244.
30 S. Y. Park, C. H. Champness and I. Shih, *J. Electron. Spectrosc.*, 2015, **205**, 23–28.
31 L. Silipigni, L. Schirò, L. M. Scolaro, G. D. Luca and G. Salvato, *Appl. Surf. Sci.*, 2011, **257**, 10888–10892.
32 L. L. Luo, F. S. Li, H. C. Zhang, Y. Z. Duan and W. C. Wang, *Sep. Purif. Technol.*, 2023, **323**, 124485.
33 D. Kołodyńska, D. Fila and Z. Hubicki, *Chem. Eng. Process.*, 2020, **147**, 107767.
34 L. Zhang, H. Y. Jin, C. H. Shen and S. J. Gao, *Chem. Phys.*, 2020, **532**, 110594.
35 H. Wang, F. X. Yin, G. R. Li, B. H. Chen and Z. Q. Wang, *Int. J. Hydrogen Energy*, 2014, **39**, 16179–16186.
36 J. Gurgul, K. Łątka, I. Hnat, J. Rynkowski and S. Dzwigaj, *Micropor. Mesopor. Mat.*, 2013, **168**, 1–6.
37 T. Yamashita and P. Hayes, *Appl. Surf. Sci.*, 2008, **254**, 2441–2449.
38 K. I. Maslakov, Y. A. Teterin, S. V. Stefanovsky, S. N. Kalmykov, A. Y. Teterin, K. E. Ivanov and S. S. Danilov, *J. Non-Cryst. Solids*, 2018, **482**, 23–29.
39 L. Wang, T. Shinohara and B. P. Zhang, *Appl. Surf. Sci.*, 2010, **256**, 5807–5812.
40 S. Attavar, M. Diwekar, M. R. Linford, M. A. Davis and S. Blair, *Appl. Surf. Sci.*, 2010, **256**, 7146–7150.
41 B. Zhang, Y. Cao, S. T. Li, Z. Jiang, G. W. He and H. Wu, *J. Membr. Sci.*, 2016, **518**, 243–253.
42 P. Piotrowski, A. Krogul-Sobczak and A. Kaim, *J. Environ. Chem. Eng.*, 2019, **7**, 103147.
43 J. Bassil, S. Roualdès, V. Flaud and J. Durand, *J. Membr. Sci.*, 2014, **461**, 1–9.